Journal of Magnetic Resonance 193 (2008) 251–258

Contents lists available at ScienceDirect

Journal of Magnetic Resonance

journal homepage: www.elsevier.com/locate/jmr

Solid-state NMR adiabatic TOBSY sequences provide enhanced sensitivity for multidimensional high-resolution magic-angle-spinning ^{1}H MR spectroscopy ☆

Ovidiu C. Andronesi [a,b,*], Dionyssios Mintzopoulos [a,b], Jochem Struppe [c], Peter M. Black [d], A. Aria Tzika [a,b,*]

[a] NMR Surgical Laboratory, Department of Surgery, Massachusetts General Hospital and Shriner's Burn Institute, Harvard Medical School, 51 Blossom Street, Room 261, Boston, MA 02114, USA
[b] Athinoula A. Martinos Center of Biomedical Imaging, Department of Radiology, Massachusetts General Hospital, Boston, MA 02114, USA
[c] Bruker BioSpin Corp, Billerica, MA 01821, USA
[d] Department of Neurosurgery, Brigham and Women's Hospital, Harvard Medical School, Boston, MA 02115, USA

ARTICLE INFO

Article history:
Received 6 February 2008
Revised 12 May 2008
Available online 27 May 2008

Keywords:
Total through bond correlation spectroscopy (TOBSY)
Total correlation spescroscopy (TOCSY)
High-resolution magic-angle-spinning (HRMAS)
Adiabatic inversion pulses (AIP)
Glioblastoma multiforme (GBM)

ABSTRACT

We propose a solid-state NMR method that maximizes the advantages of high-resolution magic-angle-spinning (HRMAS) applied to intact biopsies when compared to more conventional liquid-state NMR approaches. Theoretical treatment, numerical simulations and experimental results on intact human brain biopsies are presented. Experimentally, it is proven that an optimized adiabatic TOBSY (TOtal through Bond correlation SpectroscopY) solid-state NMR pulse sequence for two-dimensional ^{1}H–^{1}H homonuclear scalar-coupling longitudinal isotropic mixing provides a 20%–50% improvement in signal-to-noise ratio relative to its liquid-state analogue TOCSY (TOtal Correlation SpectroscopY). For this purpose we have refined the $C9^1_{15}$ symmetry-based ^{13}C TOBSY pulse sequence for ^{1}H MRS use and compared it to MLEV-16 TOCSY sequence. Both sequences were rotor-synchronized and implemented using WURST-8 adiabatic inversion pulses. As discussed theoretically and shown in simulations, the improved magnetization-transfer comes from actively removing residual dipolar couplings from the average Hamiltonian. Importantly, the solid-state NMR techniques are tailored to perform measurements at low temperatures where sample degradation is reduced. This is the first demonstration of such a concept for HRMAS metabolic profiling of disease processes, including cancer, from biopsies requiring reduced sample degradation for further genomic analysis.

1. Introduction

High-resolution magic-angle-spinning (HRMAS) ^{1}H nuclear magnetic resonance spectroscopy (^{1}H MRS) is a promising tool for metabolic profiling [1–3] since it can be used to study unprocessed tissue in a non-destructive manner. Compared to the well-known imaging methods of histopathology and MRI that detect mostly morphological changes, ^{1}H MRS is sensitive to the tissue chemistry and can be used to differentiate metabolic phenotypes. Hence, it can increase specificity and accuracy of diagnostic methods. Due to its increased resolution, ex-vivo HRMAS ^{1}H MRS is a helpful tool in explaining and assigning in-vivo ^{1}H MRS spectra.

Although, magic-angle-spinning (MAS) has been adopted from solid-state nuclear magnetic resonance (NMR) as a line-narrowing technique that reduces magnetic susceptibility differences and averages out anisotropic interactions such as chemical shielding anisotropy (CSA) or dipolar couplings (D) for samples that are not purely isotropic liquids, this has not been followed by the use of solid-state pulse sequences. Currently, HRMAS ^{1}H MRS on tissue biopsies employs conventional liquid-state pulse sequences and assumes that MAS alone is sufficient to remove the residual anisotropic interactions present in partially immobilized samples. While this holds true for simple one-dimensional (1D) ^{1}H MRS, in multidimensional experiments that rely on ^{1}H–^{1}H homonuclear scalar-coupling (*J*-coupling) mediated magnetization-transfer (i.e., TOtal Correlation SpectroscopY or TOCSY) residual anisotropic interactions can be reintroduced [4] unintentionally by pulse sequences not designed to eliminate them.

☆ O.C.A., D.M. and A.A.T. initiated the project. O.C.A and A.A.T. designed the experiments and methods. O.C.A. and D.M. performed experiments. J.S. assisted with the implementation of the methods. P.M.B. supplied biopsies. O.C.A. analyzed the data and drafted the initial manuscript, and all authors contributed to subsequent revisions.

* Corresponding authors. Addresses: Athinoula A. Martinos Center of Biomedical Imaging, Department of Radiology, Massachusetts General Hospital, Harvard Medical School, 149 Thirteenth Street, Suite 2301, Charlestown, MA 02129, USA. Fax: +1 617 726 7422 (O.C. Andronesi); NMR Surgical Laboratory, Department of Surgery, Massachusetts General Hospital and Shriner's Burn Institute, Harvard Medical School, 51 Blossom Street, Room 261, Boston, MA 02114, USA. Fax: +1 617 720 3544 (A.A. Tzika).

E-mail addresses: ovidiu@nmr.mgh.harvard.edu (O.C. Andronesi), aaria_tzika@hms.harvard.edu (A.A. Tzika).

1090-7807/$ - see front matter © 2008 Elsevier Inc. All rights reserved.
doi:10.1016/j.jmr.2008.05.017

Therefore, the transfer efficiency can be dramatically altered, resulting in decreased sensitivity. At the same time, undesired transfer through residual dipolar couplings can lead to through-space intra- or inter-molecular correlations that compromises metabolite assignment. Enhancing signal-to-noise ratio (SNR) and quality of assignment are crucial for HRMAS ^{1}H MRS in order to become successful and have a wide spread use in tissue biopsies characterization.

Multidimensional spectroscopy is, however, necessary for unambiguous assignment and quantification of metabolites present in "crowded" and overlapping 1D spectra. Recent advances in solid-state NMR [5], based on symmetry principles and average Hamiltonian theory (AHT), allow the design of pulse sequences that cancel the 1st order average Hamiltonian and minimize the higher orders contributions from CSA, D and offset terms, maintaining only the isotropic *J*-coupling. These sequences, known as TOBSY (TOtal through Bond correlation SpectroscopY), were originally developed for ^{13}C spectroscopy [6,7] and have been demonstrated in immobilized systems [6–9], or more recently were successfully used to study dynamics and structure of membrane proteins [10] in lipid bilayers or protein fibrils [11]. A few HRMAS ^{1}H NMR studies on polymers and other organic compounds [12,13] have used TOBSY sequences, albeit without the use of adiabatic pulses and their superior performance. Moreover, the benefit of *J*-only TOCSY sequences has been recognized in the absence of MAS for liquid-state NMR studies of partially alligned proteins [14].

Tissue biopsies have properties that are closely mimicked by proteoliposome samples [10]. Hence, a similar approach for HRMAS ^{1}H MRS on tissue biopsies would prove beneficial for: (1) improved detection of relevant tissue biomarkers of high-molecular-weight and reduced mobility (e.g. phospholipids), (2) detection of new macromolecular biomarkers such as proteins, glycolipids, or lipoproteins, and (3) use of low temperatures (<−5 °C) and MAS rates (<3 kHz) to preserve sample integrity for further gene expression analysis [15]. At low temperatures, residual anisotropic interactions increase due to slower molecular dynamics, making "well-designed" sequences even more important. To date, all HRMAS experiments have been carried out at temperatures above 0 °C. Using solid-state NMR principles, a new class of experiments can be developed that would provide information that is not usually attainable from liquid-state NMR. Particularly, at low temperatures the tissues might be clamped in a certain metabolic state of interest. In addition to reduced sample degradation or metabolic clamping, HRMAS ^{1}H MRS experiments at lower temperatures could be combined with dynamic nuclear polarization (DNP) [16,17] for further signal enhancement.

We have adapted the $C9^1_{15}$ (TOBSY) symmetry-based pulse sequence [5,8,9] for 2D HRMAS ^{1}H MRS and compared the magnetization-transfer efficiency and SNR to MLEV-16 (TOCSY, [18]) on brain biopsy specimens. We employed, in both cases, WURST-8 [19] radio-frequency (r.f.) adiabatic inversion pulses (AIP) for their efficient use of r.f. power to compensate pulse offsets, inhomogeneity and miscalibration with reduced r.f. heating. By design and symmetry constraints, $C9^1_{15}$ (Fig. 1) is a rotor-synchronized sequence with a fixed WURST-8 pulse length to rotor period ratio of 15/18, according to the WiW scheme [9]. To compare results under similar conditions, the adiabatic MLEV-16 [20] was rotor-synchronized as previously proposed [21], by making the WURST-8 pulse length equal to one rotor period. The WURST-8 pulse for $C9^1_{15}$ is slightly shorter than its MLEV-16 analogue, requiring a small increase in the peak r.f. field for the same bandwidth and adiabaticity factor. As discussed in the following, we also compared the situations where the WURST-8 pulses have the same duration for both sequences and found a similar gain factor. In the following

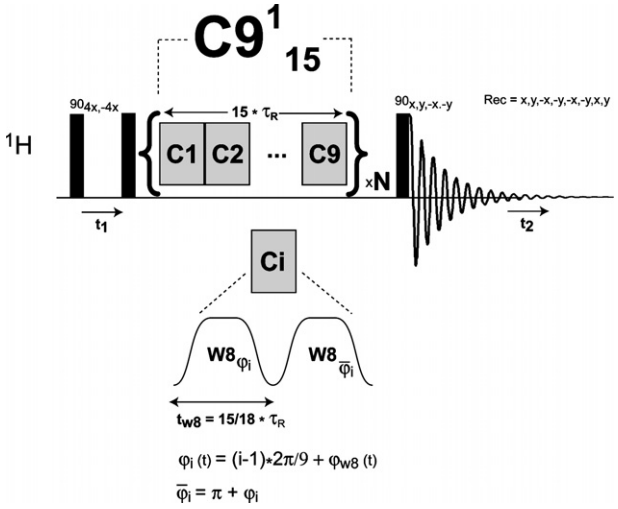

Fig. 1. 2D [^{1}H,^{1}H] TOBSY experiment employing an adiabatic $C9^1_{15}$ pulse sequence. Nine C elements ("C", grey boxes) span 15 rotor periods (τ_R). The block of nine C elements is repeated several times (N) for the desired mixing duration. Each C element is constructed according to the WiW scheme [9] from two back-to-back and 180° phase-shifted WURST-8 adiabatic inversion pulses (W8). The phases φ_i are calculated according to the overall *C*9 symmetry and internal WURST-8 phase modulation.

when referring to $C9^1_{15}$ or MLEV-16 we will mean adiabatic rotor-synchronized sequences.

2. Theory

The time-dependent Hamiltonian in the rotating frame of a homonuclear two-spins system, which is subjected to periodic perturbation of the magic-angle-spinning (t_{MAS}), r.f. amplitude- (t_{AM}) and phase- (t_{PM}) modulation, can be expressed as:

$$\begin{aligned}\widehat{H}(t_{MAS},t_{AM},t_{PM}) = &-\Omega_1\widehat{I}_{1z} - \Omega_2\widehat{I}_{2z} - S\omega_0[\hat{\sigma}_1(t_{MAS})\widehat{I}_{1z} \\ &+ \hat{\sigma}_2(t_{MAS})\widehat{I}_{2z}] + S\frac{\gamma^2\hbar^2}{2r_{12}^3}[1-3\cos^2\theta_{12}(t_{MAS})] \\ &\times(3\widehat{I}_{1z}\widehat{I}_{2z} - \widehat{I}_1\widehat{I}_2) + 2\pi J_{12}\widehat{I}_1\widehat{I}_2 + \omega_1(t_{AM})[\widehat{F}_x \\ &\times\cos\varphi(t_{PM}) + \widehat{F}_y\sin\varphi(t_{PM})] \qquad (1)\end{aligned}$$

where $\Omega_{1,2}$ represent resonance offsets; ω_0 Larmor frequency; $\hat{\sigma}_{1,2}$ CSA tensors; r_{12} internuclear distance; θ_{12} angle between internuclear vector and static B_0 field; S order parameter [22,23] ($S\in[0,1]$ models external or internal molecular dynamics, $S=0$ for purely isotropic liquids and $S=1$ for rigid solids); J_{12} isotropic scalar-coupling; ω_1 r.f. amplitude; φ r.f. phase; $\widehat{I}_{1,2}$ single spin operators; $\widehat{F}_{1,2}$ two-spins operators. For our purpose only the homonuclear dipolar- and scalar-couplings were considered (fourth and fifth term). Heteronuclear couplings were not included either because of the natural abundance ^{13}C in biopsy samples, or because they can be decoupled.

Due to periodic time-dependence, the average Hamiltonian theory [24] can be used to calculate the spin evolution. Using rank 2 irreducible spherical tensors [25] the Hamiltonian is transformed first in the interaction frame ($\widehat{\widehat{H}}$) of the r.f. field. In Levitt's notation [5], this can be decomposed as:

$$\widehat{\widehat{H}} = \sum_{\Lambda}\sum_{m=-l}^{l}\sum_{\mu=-\lambda}^{\lambda}\widehat{\widehat{H}}^{\Lambda}_{lm\lambda\mu} \qquad (2)$$

where $l=\overline{0,2}$ and $\lambda=\overline{0,2}$ represent the space- and spin-ranks, respectively, of the spin interactions Λ (CSA, D, J), and m and μ are the space and spin quantum numbers.

As a result of interference between MAS and r.f. field in averaging the NMR interactions, a general CN_n^v symmetry-based pulse sequence will select in the lowest-order average Hamiltonian the interactions that satisfy the following condition:

$$mn - \mu v = kN \tag{3}$$

For TOBSY [6–9] sequences the only desired interaction is the J scalar-coupling that has the components $\{l,m,\lambda,\mu\} = \{0,0,0,0\}$. This means that Eq. (3) must be only satisfied for $m = \mu = k = 0$, since all other interactions have different $\{l,m,\lambda,\mu\}$ components. This leads to one possible series of TOBSY sequences based on the $C9^1_{9p\pm3}$ symmetry [9].

MLEV-16 used in liquid-state NMR for TOCSY [20,26,27] does not have such a selection mechanism for anisotropic interactions and compensates only for the resonance offsets. This makes MLEV-16 sensitive to dipolar couplings or CSA in samples that are not purely liquids. In order to visualize better the theoretical behavior of $C9^1_{15}$ and MLEV-16 sequences, numerical simulations have been employed, as described below.

3. Methods

3.1. Numerical simulations

Prior to measurements, we performed quantum mechanical numerical simulations to predict the magnetization-transfer buildups of $C9^1_{15}$ and MLEV-16. The simulations were performed in the GAMMA [28] environment assuming a two-spin (protons) system described by the Hamiltonian of Eq. (1) with a scalar-coupling of 10 Hz and offsets of ±1500 Hz (±2.5 ppm at 600 MHz ^{1}H) or dipolar couplings of 70 Hz (corresponding to an order parameter $S = 0.01$ for vicinal protons at a distance of 2.5 Å), 2100 Hz ($S = 0.3$) and 7000 Hz ($S = 1$). These conditions can be easily met when working with tumor biopsies. In particular, the size of dipolar couplings may increase when molecular mobility is reduced, as it is expected for macromolecules (lipids, phospholipids and peptides) involved in tumor metabolism, or as occurs at low temperatures. The CSA of protons is typically very small and was not considered. Results of simulations are shown in Figs. 2(a–d) and 3(a and b).

In all simulations spin evolution was calculated using the piecewise constant Hamiltonian approach [29]. The initial density matrix was set $\hat{I}_{1z}$ and the detect operator was considered to be $\hat{I}_{2z}$. Simulations have been performed for an MAS rate of 3 kHz. Each WURST-8 pulse was discretized in 200 steps as in the experimental implementation (*vide infra*). The maximum r.f field for WURST-8 pulses was 14.5 kHz in the case of $C9^1_{15}$ and 12 kHz for MLEV-16. Other adiabatic inversion pulses [30–32] were investigated and gave similar results. The periodic nature of each sequence was exploited to speed up calculations for long mixing times. The propagator corresponding to one sequence cycle was used repeatedly (15 rotor periods for $C9^1_{15}$ and 16 rotor periods for MLEV-16). 120 different powder orientations were integrated according to a non-random numerical method [33].

3.2. Experimental procedures

3.2.1. Brain biopsies and sample preparation

We recorded control spectra of brain biopsy samples from four patients (undergoing surgery for epilepsy), with sample weights of 9.2, 19.3, 20 and 24.5 mg. Spectra were also recorded from brain cancer biopsy samples collected from six patients that had undergone surgery for glioblastoma multiforme (GBM), with sample weights of 10, 11.2, 12.6, 17.3, 18.8 and 22.7 mg. First, 10 μl of 3-(trimethylsilyl)-propionic acid-D4 (TSP) standard (50 mM in D_2O) was introduced into the 4 mm ZrO_2 rotors before biopsies for referencing and field locking. The samples were secured and tightened in the rotors with a top insert, screw and cap (Bruker).

3.2.2. NMR experiments

All NMR experiments were conducted on a wide-bore Bruker Avance spectrometer (600 MHz, ^{1}H) using a 4 mm double channel HRMAS probehead (Bruker) equipped with a deuterium lock channel. All measurements were made at 3 kHz MAS and −8 °C (the minimum temperature possible with our setup for 3 kHz MAS).

The 2D [^{1}H,^{1}H] TOBSY experiment, which employs the adiabatic $C9^1_{15}$ pulse sequence, is shown in Fig. 1. Nine C elements (grey boxes) span 15 rotor periods (τ_R). Each C element is constructed according to the WiW scheme [9] from two back-to-back and 180° phase-shifted WURST-8 (W8) adiabatic inversion pulses ($\omega_1(t) = \omega_{1,\max}(1 - |\sin(t\pi/T_p)|^8)$, T_p the pulse length). The WURST-8 pulse has a length of 277.78 μs at 3 kHz MAS, requiring a peak r.f. field ($\omega_{1,\max}$) of 14.5 kHz for an adiabaticity factor of 5. The phases of each C element are calculated according to the overall $C9$ symmetry and internal WURST-8 phase modulation ($\varphi_i(t) = 2\pi i/N + (\omega_{1,\max})^2/2Q_0(t - T_p/2)^2, i = \overline{0,8}, Q_0$ quality factor). The WURST-8 shape was discretized in 200 steps in order to efficiently use the memory buffer and was calculated using the Shape Tool in XWINNMR 3.5 (Bruker). The block of nine C elements is repeated an integer number (N) of times for the desired mixing duration. Rectangular 90° hard pulses (8 μs) pulses were used to complete the 2D experiment (black rectangles in Fig. 1). Phase cycling of the first and last 90° hard pulses is given for longitudinal isotropic mixing and phase sensitive spectra recording. The pulse sequence is preceded by a water suppression block with continuous-wave (CW) low-power on-resonance irradiation (omitted from this diagram). The correct generation of the pulse sequence and WURST-8 pulses was tested with a Tektronix TDS3044B digital oscilloscope.

For the 2D [^{1}H,^{1}H] TOCSY experiment the $C9^1_{15}$ mixing block in Fig. 1 was replaced by the MLEV-16 scheme. Each 180° pulse of the MLEV-16 was constructed from a rotor-synchronized WURST-8 adiabatic pulse, as previously proposed [21]. At the 3 kHz MAS rate the WURST-8 pulse length for MLEV-16 is 333.33 μs, requiring a maximum r.f. field of 12 kHz for an adiabaticity factor of 5. This is a slightly lower field than in the case of $C9^1_{15}$. To eliminate the possibility that the advantage of $C9^1_{15}$ is due to higher r.f. field, MLEV-16 was also performed at 3.6 kHz MAS rate. Running MLEV-16 at 3.6 kHz MAS requires the same r.f. field (14.5 kHz) as $C9^1_{15}$ at 3 kHz MAS. Experimental results and simulations are presented in Fig. 6.

In all experiments, identical acquisition and processing parameters were used. These parameters were as follows: 2k points along the direct dimension (13 ppm spectral width), 200 points along the indirect dimension (7.5 ppm spectral width), 8 scans, 2 dummy scans, 1s CW low-power on-resonance water presaturation, 2s total repetition time, 45 ms mixing time (maximum buildup signal for most of the metabolites), 56 min total acquisition time; QSINE = 3 window function in both dimensions, FT with 2k points in the direct dimension and zero-filling to 1k in the second dimension, phase correction in both dimensions and baseline correction in the second dimension. Acquisition and processing of spectra were completed using XWINNMR 3.5 software (Bruker).

4. Results

Simulated buildup curves of $C9^1_{15}$ (black) compared to MLEV-16 (red) predict improved magnetization-transfer of $C9^1_{15}$ with regard to both the offset (Fig. 2a) and the size of dipolar couplings (Fig. 2b–d), indicating that $C9^1_{15}$ can more than double the transfer efficiency of MLEV-16. Fig. 2a shows that even in the absence of dipolar couplings ($S = 0$) the $C9^1_{15}$ performs better than MLEV-16

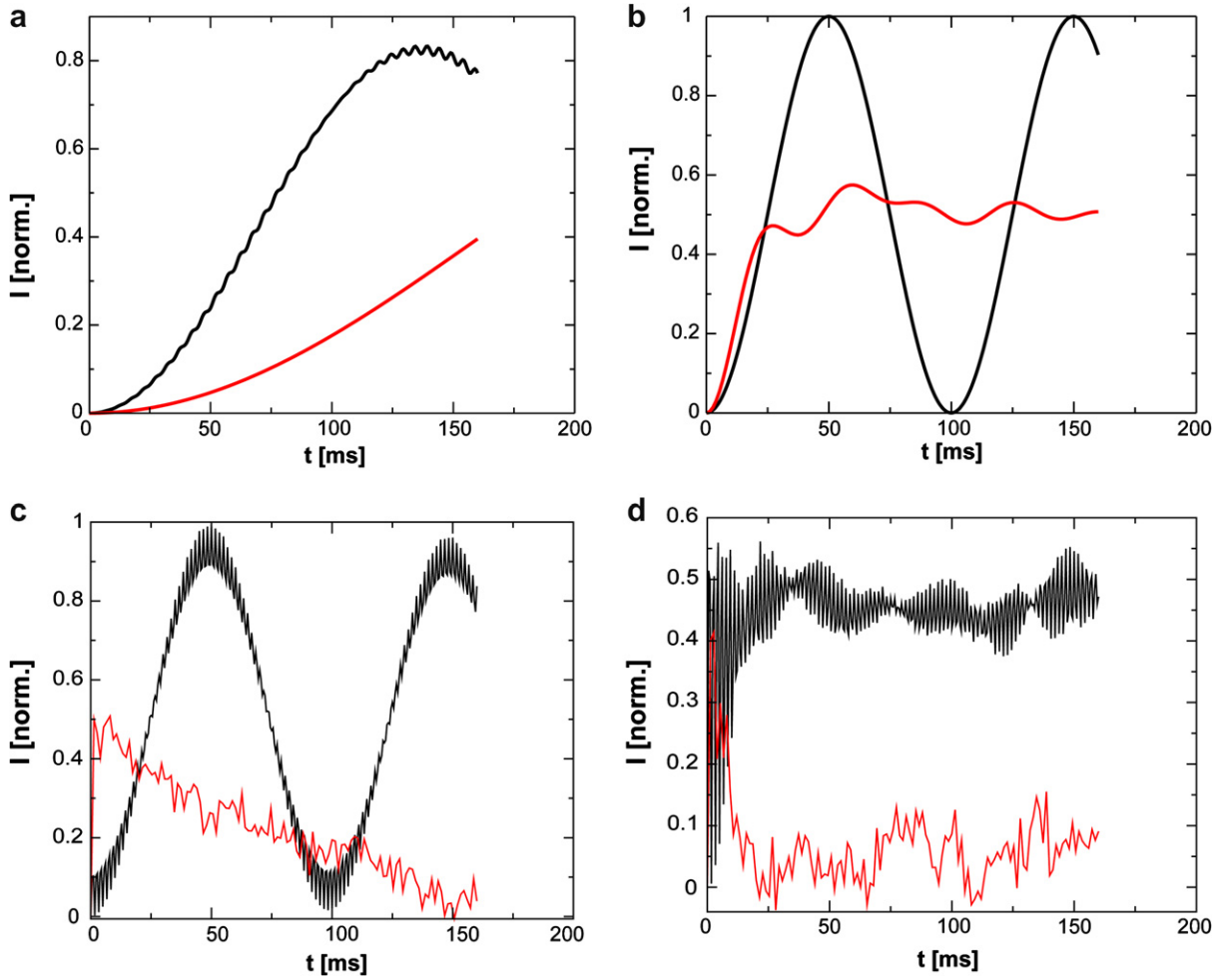

Fig. 2. Numerical simulations of magnetization-transfer buildups via a scalar-coupling of 10 Hz under adiabatic $C9^1_{15}$ (black) or adiabatic MLEV-16 (red) mixing. (a) An offset of ± 2.5 ppm (at 600 MHz ^{1}H), or dipolar couplings of (b) 70 Hz (order parameter $S = 0.01$), (c) 2100 Hz ($S = 0.3$) and (d) 7000 Hz ($S = 1$) are considered for two vicinal protons at 2.5 Å distance. MAS of 3 kHz is assumed in all simulations. WURST-8 maximum r.f fields of 14.5 kHz ($C9^1_{15}$) and 12 kHz (MLEV-16) are employed.

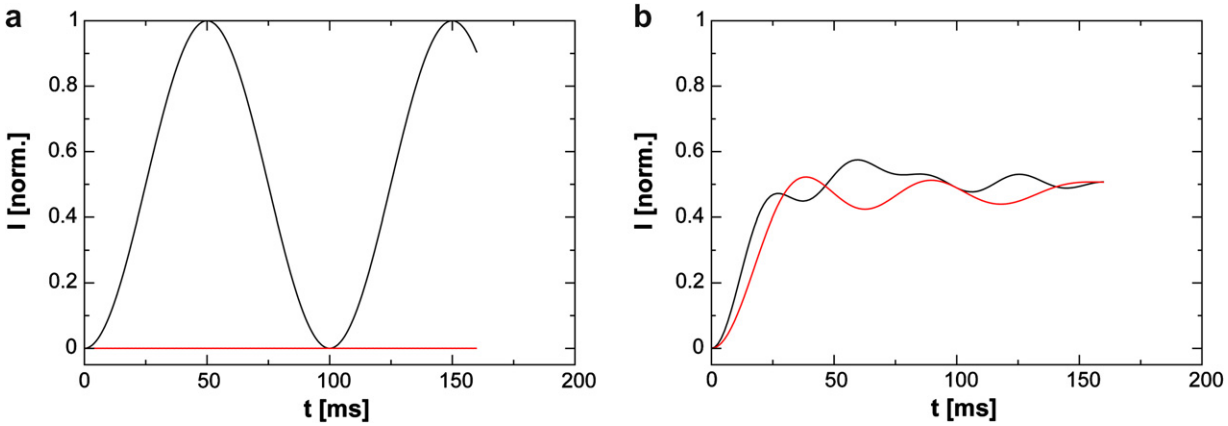

Fig. 3. The contribution of dipolar couplings in $C9^1_{15}$ (a) and MLEV-16 (b) transfers. An order parameter of $S = 0.01$ has been considered in all cases and the scalar-coupling was set to $J = 10$ Hz (black) or $J = 0$ Hz (red).

for the offsets and chemical shifts dispersion characteristic for protons. When dipolar couplings are introduced, MLEV-16 performs gradually worse than $C9^1_{15}$ with increasing order parameters (Fig. 2b–d). For large order parameters ($S \sim 1$) MLEV-16 fails completely. At small order parameter ($S = 0.01$), the marked effect of dipolar couplings on MLEV-16 can be shown in simulations where the scalar-coupling is set to 0. In Fig. 3b buildups of MLEV-16 with $J = 10$ Hz (black) and $J = 0$ Hz (red) are compared. As can be seen, the two buildups are similar and suggest that the transfer is in fact largely given by the dipolar couplings. Power averaging of the orientation dependent dipolar couplings makes the buildup to not reach the maximum value of one as in the case of isotropic sca-

lar-coupling. A further consequence of the dipolar transfer is that the TOCSY spectra will contain not only through bond correlations but also through-space contacts, complicating the assignment. By contrast, the buildups of $C9^1_{15}$ in Fig. 3a show no transfer for $J = 0$ Hz (red), reassuring that the entire transfer is due to the scalar-couplings ($J = 10$ Hz, black).

Representative 2D NMR spectra of control and tumor (GBM) specimens obtained with the $C9^1_{15}$ (black) and MLEV-16 (red) sequences are shown in Fig. 4. The most striking difference between specimens is the overwhelming presence of lipids in the GBM spectra accompanied by the lack of *N*-acetyl-aspartate (NAA), γ-amino butyric acid (GABA) and aspartate (Asp).

The improved transfer efficiency of $C9^1_{15}$ is better illustrated by comparing 1D slices of several relevant metabolites (lactate (Lac), NAA, glycerophosphocholine (GPC), and polyunsaturated fatty acids (PUFA)) that were extracted along the indirect dimension from the 2D spectra (Fig. 4). The peaks in 1D slices were integrated (using MestReC software [34]), and as shown in Fig. 5, $C9^1_{15}$ is superior to MLEV-16 for both small- (Lac, NAA) and large- (GPC, PUFA) molecular-weight metabolites.

The 2D SNR gain fraction SNR_{C9}/SNR_{MLEV16} was further calculated for each individual sample. 2D spectra were quantified using Sparky program (T.D. Goddard and D.G. Kneller, SPARKY 3, UCSF). The SNR gains were then averaged (mean ± SEM) over the number of samples. Student's *t*-test *p*-values were computed against the null hypothesis of no SNR gain (fraction equal to 1). Table 1 summarizes the gain in SNR for $C9^1_{15}$ relative to MLEV-16 for 2D cross-peak volumes of selected metabolites. A significant SNR gain of approximately 50% was calculated for larger, slower-tumbling metabolites such as GPC and PUFA, while a lower but still detectable SNR gain close to 20% was obtained for low-molecular-weight, faster-tumbling metabolites (i.e., NAA and Lac).

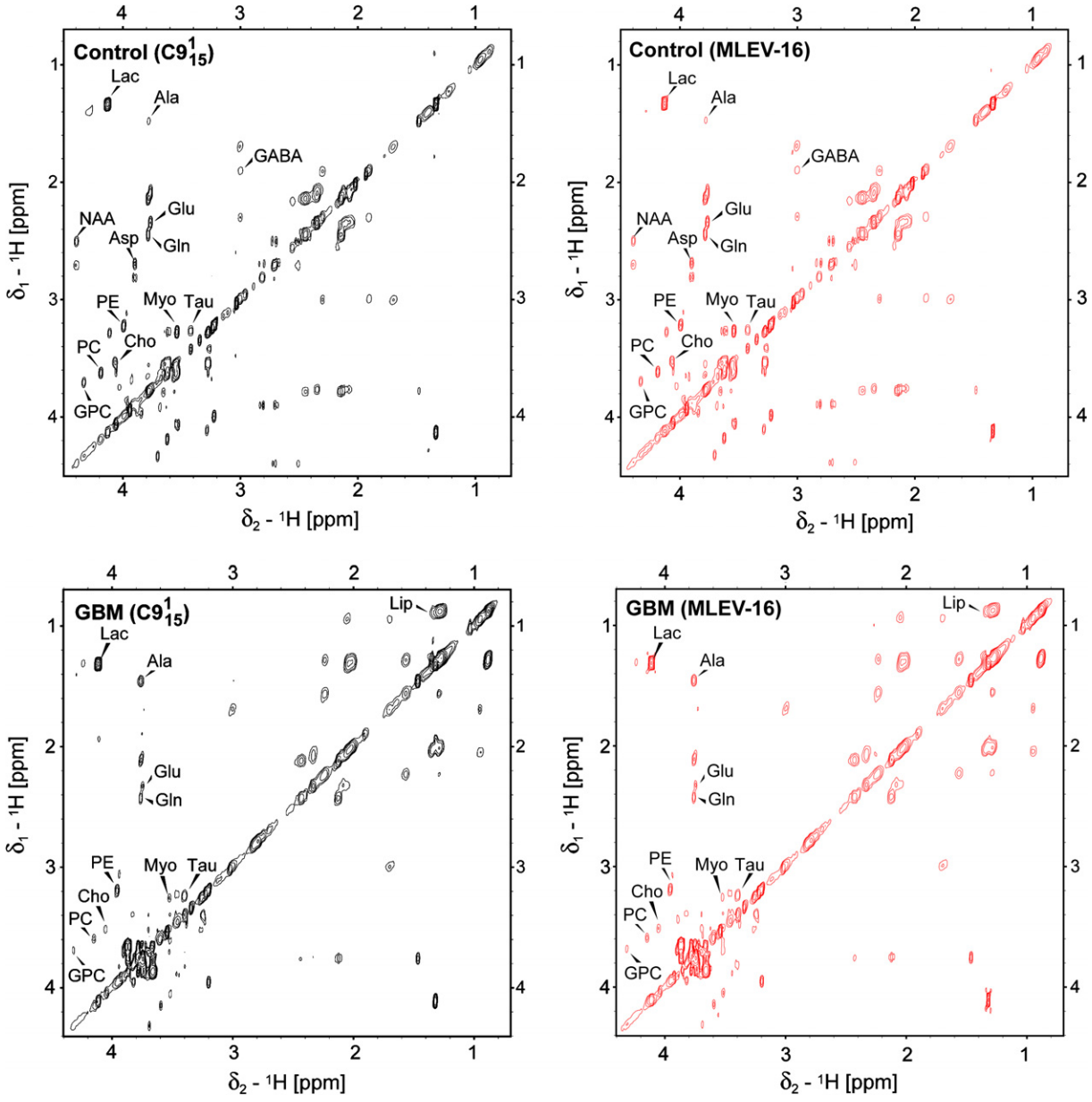

Fig. 4. 2D [^{1}H,^{1}H] HRMAS MR spectra of control and glioblastoma multiforme (GBM) brain biopsy samples which were acquired with adiabatic $C9^1_{15}$ (left) and adiabatic MLEV-16 (right) at 3 kHz MAS, −8 °C and 600 MHz ^{1}H. Assigned metabolites: Alanine (Ala), γ-amino-butyric acid (GABA), Choline (Cho), Glutamine (Gln), Glutamate (Glu), Glycerophosphocholine (GPC), Lipids (Lip), Myoinositol (Myo), *N*-acetyl-aspartate (NAA), Phosphocholine (PC), Phosphoethanolamine (PE), and Taurine (Tau). Similar contours are chosen, and the lower threshold is 10-fold the noise level.

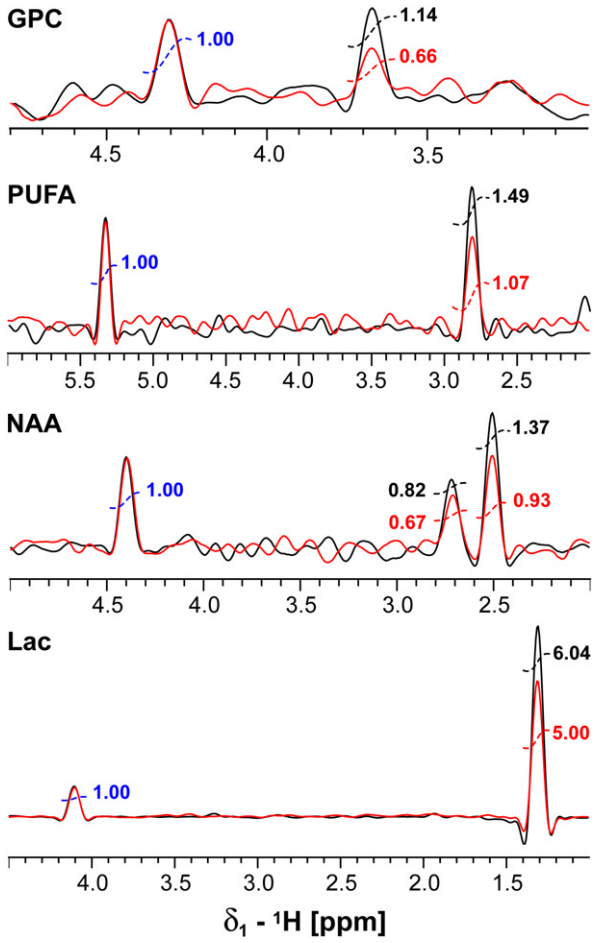

Fig. 5. 1D slices along the indirect dimension of the 2D spectra (Fig. 4) recorded with adiabatic $C9^1_{15}$ (black) and adiabatic MLEV-16 (red). Integral values are given with diagonal peaks normalized to 1.

Table 1
2D SNR gain of $C9^1_{15}$ relative to MLEV-16 (SNR_{C9}/SNR_{MLEV16}) for relevant metabolites

Metabolite	$\delta1/\delta2$ (ppm)	SNR gain (mean ± SEM, %)	Biopsies (#/type)	Student's *t*-test (*P*-values)
GPC	3.68/4.32	55 ± 13	3/GBM	0.050
PUFA	2.81/5.33	42 ± 14	4/GBM	0.005
NAA	2.51/4.39	36 ± 14	4/Controls	0.012
Lac	1.33/4.13	18 ± 3	6/GBM	0.008

5. Discussion

The present study demonstrates that merging concepts from solid- and liquid-state NMR can improve detection conditions for complex biological samples such as tissue biopsies. The novelty of our proposal lies in introducing and refining the TOBSY concept, used to obtain ^{13}C through bond correlations in solid-state NMR, for the purpose of 2D HRMAS ^1H MRS on tissue biopsies. The benefits of this combined approach can be both quantitative, by increasing signal-to-noise, and qualitative, by allowing identification of new biomarkers.

Here, we focused more on the quantitative aspect and showed that enhanced sensitivity can be obtained. This result is valid for large molecules (phospholipids), as expected, but also for small metabolites (NAA, lactate). A further step is to find evidence for new tumor markers, especially larger macromolecules such as proteins or peptides that play important roles in cancer and can thus lead to a greater understanding of tumor genetics and pathology. The proposed approach can be extended also to study agonist-receptor interactions [35,36] in tissues to screen for new drug targets.

An important contribution to the efficiency of the method comes from the ability to use adiabatic pulses. We found similar advantages, such as uniform inversion profile with low r.f. power, compensate r.f inhomogeneity, reduced susceptibility for r.f. miscalibration and instrument instability in using adiabatic pulses as previously reported [9,21,27]. However, one possible cause for the improved efficiency of $C9^1_{15}$ might be the slightly higher r.f. field used during mixing period. To examine whether the superior performance of $C9^1_{15}$ was due to the small increase in r.f. amplitude of WURST-8 pulses (14.5 kHz for $C9^1_{15}$ vs. 12 kHz for MLEV-16 at 3 kHz MAS) we performed both simulations and experiments of MLEV-16 at 3.6 kHz MAS. Running MLEV-16 at 3.6 kHz MAS requires the same r.f. field (14.5 kHz) as $C9^1_{15}$ at 3 kHz. Fig. 6 demonstrates that the advantages of $C9^1_{15}$ are still preserved even when MLEV-16 is performed at higher spinning rates.

A critical aspect is also the variability for 2D metabolite quantification due to experimental bias. This can be estimated and compared if SNR is calculated separately for $C9^1_{15}$ and MLEV-16 across all samples (mean ± SEM). The measure for variability was taken as the ratio of SEM/mean (%). Table 2 indicates that less variability is observed when using the adiabatic $C9^1_{15}$ sequence.

To this point, we need to note that although the observed SNR gain was significant, it was lower than expected from simulations of the two-spin system under ideal conditions (i.e. neglecting relaxation). Experimentally this might be due to a variety of factors, such as T1 relaxation in the rotating frame during r.f. mixing, multispin effects, or slight errors in generation of the adiabatic pulse that accumulate over the mixing time.

The gain in SNR is expected to increase in conditions where samples are more rigid, for instance at lower temperatures. The possible use of lower temperatures is also justified because of the need to protect the samples from degradation. Surgical biopsies are usually frozen immediately to be preserved, hence, an NMR method that does not warm (>0 °C) them would probably be desired. Moreover, at low temperatures the tissue biopies can be clamped in a certain metabolic state of interest or can be subjected to DNP in solid-state [37,38] for considerable signal enhancement. DNP is already employed to produce hyperpolarized ^{13}C contrast agents in frozen solutions that are subsequently melted and injected for medical use in MRI or MRS [39,40]. However, such a DNP procedure would not be feasible to implement for tissue biopsies and would completely destroy the specimen. A similar approach in solid-state that preserves sample integrity would be preferable. Although, currently DNP in solid-state requires conditions [37,38] that render proton lines very broad, further advancements in this field coupled with very fast MAS [41] and optimized pulse sequences as proposed herein could increase sensitivity for ^1H MRS by several orders of magnitude. Ultimately, we envision that the achieved sensitivity may be sufficient for single scan multidimensional NMR spectroscopy [42] and lead to ultra-fast (s), multidimensional proton spectroscopy of tissue biopsies or other samples of interest. We suggest that such a development could turn the HRMAS ^1H MRS in a high throughput technique for research applications and clinical use.

6. Conclusion

In conclusion, use of solid-state TOBSY sequences, such as $C9^1_{15}$, allowed us to obtain enhanced HRMAS ^1H MRS sensitivity in mul-

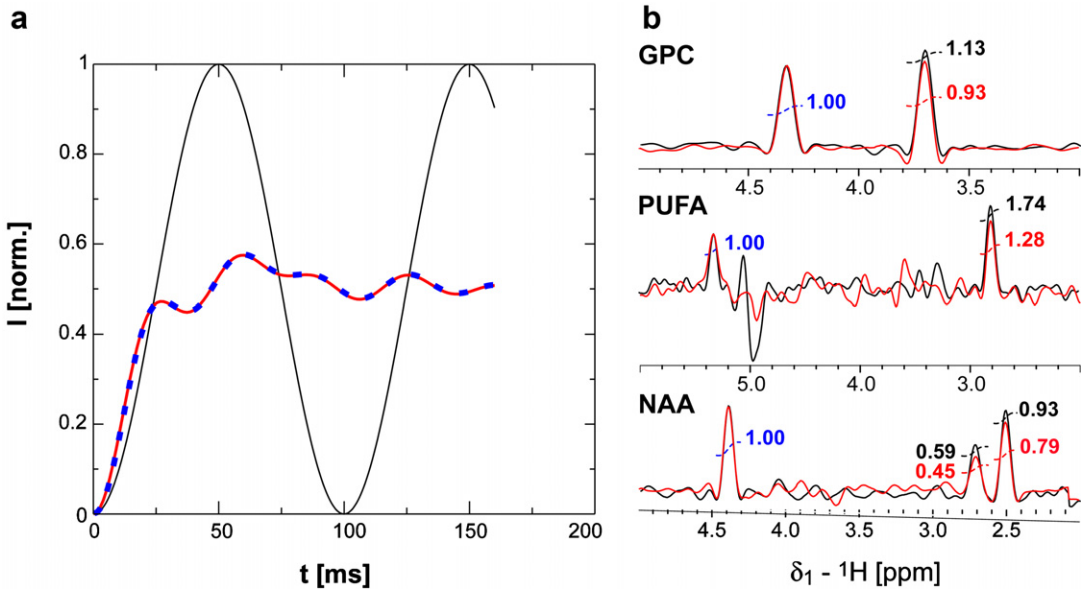

Fig. 6. Numerical simulations and experimental results for adiabatic MLEV-16 at 3.6 kHz MAS. Running MLEV-16 at 3.6 kHz MAS requires the same r.f. field (14.5 kHz) as $C9^1_{15}$ at 3 kHz. (a) The buildups of MLEV-16 at 3.6 kHz MAS (blue, dashed line) and 3 kHz MAS (red, continuous line) are identical, and inferior to $C9^1_{15}$ buildup at 3 kHz MAS (black, continuous line). The same two-spin system from Fig. 2b was assumed. (b) 1D slices along the indirect dimension of the 2D spectra recorded with adiabatic $C9^1_{15}$ (black) at 3 kHz MAS and adiabatic MLEV-16 (red) at 3.6 kHz MAS (−8 °C and 600 ^{1}H MHz were used in both cases). Integral values are given with diagonal peaks normalized to 1.

Table 2
Variability (Δ) of 2D metabolite cross-peaks in $C9^1_{15}$ and MLEV-16 experiments

Metabolite	$\delta1/\delta2$ (ppm)	$SNRC9^1_{15}$ (mean ± SEM)	SNR MLEV-16 (mean ± SEM)	$\Delta C9^1_{15}$ (SEM/mean%)	Δ MLEV-16 (SEM/mean %)
GPC	3.68/4.32	17.33 ± 4.33	11 ± 2.81	25	26
PUFA	2.81/5.33	28.5 ± 5.75	21.25 ± 5.62	20	26
NAA	2.51/4.39	70.75 ± 18.87	55.25 ± 17.18	27	31
Lac	1.33/4.13	1003.3 ± 389.6	876 ± 357.9	38	41

tidimensional experiments on tissue biopsies. The SNR of our method was superior to those using conventional liquid-state TOCSY sequences (MLEV-16). In the case of adiabatic rotor-synchronized sequences the advantage is maintained over an MAS range, requiring similar or identical r.f fields. This method is particularly useful in low temperature experiments where samples are better protected against degradation or they can be metabolically clamped. The method may be applied to study physiological and disease processes, including cancer. Increased sensitivity will allow for shorter acquisition times, smaller sized samples and reduced variability for metabolite quantification. We suggest this method for metabolic profiling, especially for improved detection of macromolecular biomarkers in tissue biopsies and stem cells requiring reduced sample degradation for further genomic analysis. Moreover, in the broader context of life sciences our approach can be extended into structural biology (membrane proteins, protein fibrils) complementary to the existing NMR methods.

Acknowledgments

This work was supported by discretional funds to A.A.T. We thank Jerome L. Ackerman and Christian Farrar for technical assistance at the Athinoula A. Martinos Center for Biomedical Imaging, Massachusetts General Hospital, Harvard Medical School, Boston, USA.

References

[1] A.A. Tzika, L.L. Cheng, L. Goumnerova, J.R. Madsen, D. Zurakowski, L.G. Astrakas, M.K. Zarifi, R.M. Scott, D.C. Anthony, R.G. Gonzalez, et al., Biochemical characterization of pediatric brain tumors by using in vivo and ex vivo magnetic resonance spectroscopy, J. Neurosurg. 96 (2002) 1023–1031.
[2] K.K. Lehtimaki, P.K. Valonen, J.L. Griffin, T.H. Vaisanen, O.H.J. Grohn, M.I. Kettunen, J. Vepsalainen, S. Yla-Herttuala, J. Nicholson, R.A. Kauppinen, Metabolite changes in BT4C rat gliomas undergoing ganciclovir-thymidine kinase gene therapy-induced programmed cell death as studied by H-1 NMR spectroscopy in vivo, ex vivo, and in vitro, J. Biol. Chem. 278 (2003) 45915–45923.
[3] J.L. Griffin, J.P. Shockcor, Metabolic profiles of cancer cells, Nat. Rev. Cancer 4 (2004) 551–561.
[4] R.G. Griffin, Dipolar recoupling in MAS spectra of biological solids, Nat. Struct. Biol. 5 (1998) 508–512.
[5] M.H. Levitt, Advances in NMR, in: D.M. Grant, R.K. Harris (Eds.), Encyclopedia of Nuclear Magnetic Resonance, vol. 9, John Wiley & Sons Ltd., Chichester, 2002, pp. 165–196.
[6] M. Baldus, B.H. Meier, Total correlation spectroscopy in the solid state. The use of scalar couplings to determine the through-bond connectivity, J. Magn. Reson. Ser. A 121 (1996) 65–69.
[7] M. Baldus, R.J. Iuliucci, B.H. Meier, Probing through-bond connectivities and through-space distances in solids by magic-angle-spinning nuclear magnetic resonance, J. Am. Chem. Soc. 119 (1997) 1121–1124.
[8] E.H. Hardy, R. Verel, B.H. Meier, Fast MAS total through-bond correlation spectroscopy, J. Magn. Reson. 148 (2001) 459–464.
[9] E.H. Hardy, A. Detken, B.H. Meier, Fast-MAS total through-bond correlation spectroscopy using adiabatic pulses, J. Magn. Reson. 165 (2003) 208–218.
[10] O.C. Andronesi, S. Becker, K. Seidel, H. Heise, H.S. Young, M. Baldus, Determination of membrane protein structure and dynamics by magic-angle-spinning solid-state NMR spectroscopy, J. Am. Chem. Soc. 127 (2005) 12965–12974.
[11] H. Heise, W. Hoyer, S. Becker, O.C. Andronesi, D. Riedel, M. Baldus, Molecular-level secondary structure, polymorphism, and dynamics of full-length alpha-synuclein fibrils studied by solid-state NMR, Proc. Natl. Acad. Sci. USA 102 (2005) 15871–15876.
[12] K. Thieme, G. Zech, H. Kunz, H.W. Spiess, I. Schnell, Dipolar recoupling in NOESY-Type H-1–H-1 NMR experiments under HRMAS conditions, Org. Lett. 4 (2002) 1559–1562.
[13] I. Schnell, Merging concepts from liquid-state and solid-state NMR spectroscopy for the investigation of supra- and biomolecular systems, Curr. Anal. Chem. 1 (2005) 3–27.

[14] J. Klages, H. Kessler, S.J. Glaser, B. Luy, J-ONLY-TOCSY: Efficient suppression of RDC-induced transfer in homonuclear TOCSY experiments using JESTER-1-derived multiple pulse sequences, J. Magn. Reson. 189 (2007) 217–227.
[15] A.A. Tzika, L. Astrakas, H.H. Cao, D. Mintzopoulos, O.C. Andronesi, M. Mindrinos, J.W. Zhang, L.G. Rahme, K.D. Blekas, A.C. Likas, et al., Combination of high-resolution magic angle spinning proton magnetic resonance spectroscopy and microscale genomics to type brain tumor biopsies, Intl. J. Mol. Med. 20 (2007) 199–208.
[16] M. Etzkorn, S. Martell, O.C. Andronesi, K. Seidel, M. Engelhard, M. Baldus, Secondary structure dynamics, and topology of a seven-helix receptor in native membranes, studied by solid-state NMR spectroscopy, Angewandte Chemie-International Edition 46 (2007) 459–462.
[17] O.C. Andronesi, M. von Bergen, J. Biernat, K. Seidel, C. Griesinger, E. Mandelkow, M. Baldus, Characterization of Alzheimer's-like paired helical filaments from the core domain of tau protein using solid-state NMR spectroscopy, J. Am. Chem. Soc. 130 (2008) 5922–5928.
[18] M.H. Levitt, R. Freeman, T. Frenkiel, Broad-band heteronuclear decoupling, J. Magn. Reson. 47 (1982) 328–330.
[19] E. Kupce, R. Freeman, Adiabatic pulses for wide-band inversion and broad-band decoupling, J. Magn. Reson. Ser. A 115 (1995) 273–276.
[20] W. Peti, C. Griesinger, W. Bermel, Adiabatic TOCSY for C,C and H,H J-transfer, J. Biomol. NMR 18 (2000) 199–205.
[21] A.S. Zektzer, M.G. Swanson, S. Jarso, S.J. Nelson, D.B. Vigneron, J. Kurhanewicz, Improved signal to noise in high-resolution magic angle spinning total correlation spectroscopy studies of prostate tissues using rotor-synchronized adiabatic pulses, Magn. Reson. Med. 53 (2005) 41–48.
[22] G. Lipari, A. Szabo, Model-free approach to the interpretation of nuclear magnetic-resonance relaxation in macromolecules. 1. Theory and range of validity, J. Am. Chem. Soc. 104 (1982) 4546–4559.
[23] G. Lipari, A. Szabo, Model-free approach to the interpretation of nuclear magnetic-resonance relaxation in macromolecules. 2. Analysis of experimental results, J. Am. Chem. Soc. 104 (1982) 4559–4570.
[24] U. Haeberlen, Selective averaging, in: J.S. Waugh (Ed.), Advances in magnetic resonance, High Resolution NMR in Solids, Academic Press, 1976.
[25] M. Mehring, Principles of High Resolution NMR in Solids, Springer-Verlag, Berlin Heidelberg, 1983.
[26] E. Kupce, P. Schmidt, M. Rance, G. Wagner, Adiabatic mixing in the liquid state, J. Magn. Reson. 135 (1998) 361–367.
[27] E. Kupce, P.A. Keifer, M. Delepierre, Adiabatic TOCSY MAS in liquids, J. Magn. Reson. 148 (2001) 115–120.
[28] S.A. Smith, T.O. Levante, B.H. Meier, R.R. Ernst, Computer-simulations in magnetic-resonance—an object-oriented programming approach, J. Magn. Reson. Ser. A 106 (1994) 75–105.
[29] M. Baldus, Correlation experiments for assignment and structure elucidation of immobilized polypeptides under magic angle spinning, Prog. Nucl. Magn. Reson. Spectrosc. 41 (2002) 1–47.
[30] M.S. Silver, R.I. Joseph, D.I. Hoult, Selective spin inversion in nuclear magnetic-resonance and coherent optics through an exact solution of the Bloch-Riccati equation, Phys. Rev. A 31 (1985) 2753–2755.
[31] A. Tannus, M. Garwood, Adiabatic pulses, NMR Biomed. 10 (1997) 423–434.
[32] T.L. Hwang, P.C.M. van Zijl, M. Garwood, Fast broadband inversion by adiabatic pulses, J. Magn. Reson. 133 (1998) 200–203.
[33] V.B. Cheng, H.H. Suzukawa, M. Wolfsber, Investigations of a nonrandom numerical-method for multidimensional integration, J. Chem. Phys. 59 (1973) 3992–3999.
[34] J.C. Cobas, F.J. Sardina, Nuclear magnetic resonance data processing. MestRe-C: a software package for desktop computers, Conc. Magn. Reson. A 19A (2003) 80–96.
[35] S. Luca, J.F. White, A.K. Sohal, D.V. Filippov, J.H. van Boom, R. Grisshammer, M. Baldus, The conformation of neurotensin bound to its G protein-coupled receptor, Proc. Natl. Acad. Sci. USA 100 (2003) 10706–10711.
[36] A. Lange, K. Giller, S. Hornig, M.F. Martin-Eauclaire, O. Pongs, S. Becker, M. Baldus, Toxin-induced conformational changes in a potassium channel revealed by solid-state NMR, Nature 440 (2006) 959–962.
[37] C.S. Song, K.N. Hu, C.G. Joo, T.M. Swager, R.G. Griffin, TOTAPOL: a biradical polarizing agent for dynamic nuclear polarization experiments in aqueous media, J. Am. Chem. Soc. 128 (2006) 11385–11390.
[38] P.C.A. van der Wel, K.N. Hu, J. Lewandowski, R.G. Griffin, Dynamic nuclear polarization of amyloidogenic peptide nanocrystals: GNNQQNY, a core segment of the yeast prion protein Sup35p, J. Am. Chem. Soc. 128 (2006) 10840–10846.
[39] J.H. Ardenkjaer-Larsen, B. Fridlund, A. Gram, G. Hansson, L. Hansson, M.H. Lerche, R. Servin, M. Thaning, K. Golman, Increase in signal-to-noise ratio of >10,000 times in liquid-state NMR, Proc. Natl. Acad. Sci. USA 100 (2003) 10158–10163.
[40] M. Ishii, K. Emami, S. Kadlecek, J.S. Petersson, K. Golman, V. Vahdat, J.S. Yu, R.V. Cadman, J. MacDuffie-Woodburn, M. Stephen, et al., Hyperpolarized C-13 MRI of the pulmonary vasculature and parenchyma, Mag. Reson. Med. 57 (2007) 459–463.
[41] A. Samoson, T. Tuherm, J. Past, A. Reinhold, T. Anupold, N. Heinmaa, New horizons for magic-angle spinning NMR, New Tech. Solid State NMR 246 (2005) 15–31.
[42] L. Frydman, T. Scherf, A. Lupulescu, The acquisition of multidimensional NMR spectra within a single scan, Proc. Natl. Acad. Sci. USA 99 (2002) 15858–15862.